Effects of graphene/silver nanohybrid additives on electrochemical properties of magnesium-based amorphous alloy

CrossMark

Huang Lin-jun [a, *], Wang Yan-xin [a], Huang Zhen [a], Tang Jian-guo [a, *], Wang Yao [a], Liu Ji-xian [a], Jiao Ji-qing [a], Liu Jing-quan [a], Laurence A. Belfiore [b]

[a] College of Chemistry, Chemical and Environmental Engineering, Qingdao University, Qingdao 266071, China
[b] Department of Chemical and Biological Engineering, Colorado State University, Fort Collins, CO 80523, USA

HIGHLIGHTS

- Graphene/Ag nanocomposite has been prepared successfully.
- The performance of electrode is improved by surface modification.
- $Mg_{65}Ni_{27}La_8$ + 0.2 G/A exhibits a maximum discharge capacity (814 mAh g^{-1}) at room temperature.

ARTICLE INFO

ABSTRACT

Amorphous Mg–Ni–La alloys for hydrogen storage are prepared by rapid solidification. Ag nanoparticles have been deposited onto graphene sheets to form graphene/Ag (G/A) nanocomposite through solvothermal method using ethylene glycol as solvent and reducing agent. The effects of surface modification of amorphous Mg–Ni–La alloy by introduction of different contents of G/A are systematically investigated by XRD, FT-IR, SEM, TEM and conventional electrochemical tests. The results show that the discharge capacity, cycle life, discharge potential characteristics and electrochemical kinetics of the electrodes are all improved. The surface modification enhances the electrocatalytic activity of the alloy and reduces the contact resistance of the electrodes. The $Mg_{65}Ni_{27}La_8$ with 20 wt.% G/A electrode has the largest discharge capacity of 814.8 mAh g^{-1}, which is 1.33 times that of the electrode without G/A, and the best electrochemical kinetics. Further increasing of G/A content will lead to the increase of contact resistance of the electrode, resulting in the degradation of electrode performance.

© 2014 Elsevier B.V. All rights reserved.

1. Introduction

Hydrogen storage materials have attracted increasing interest for designing future clean energy systems. Among various kinds of hydrogen storage materials studied previously, Mg-based hydrogen storage alloys are extremely promising [1–3], due to their high hydrogen capacity, low specific weight and abundance. However, the practical application of Mg-based alloys is restrained by their poor hydriding/dehydriding kinetics at room temperature and their poor charge/discharge cycle stability caused by the formation of $Mg(OH)_2$ on the surface of alloys in alkaline solution. In order to overcome such disadvantages, many additives have been explored. Briefly, they can be classified into three types: (i) transition metals (TMs), such as Nb [2–4], Ti [3,5], V [3,5] and Fe [3,6,7], (ii) transition metal oxides [TMOs] with variable valence, such as Cr_2O_3 [8,9] and WO_3 [10], and (iii) carbon allotropes, such as graphite [11,12] and carbon nanotubes [13].

A few studies about influence of carbon on the characteristics of Mg-based alloys have been reported. Iwakura et al. [14–17] reported that both the discharge capacity and the charge/discharge cycle life of MgNi electrode could be improved by surface modification with 20 wt.% graphite. In contrast, Ruggeri et al. [17] found that surface modification of MgNi by ball milling the mixture of alloy and graphite for 10 h had a major deleterious effect on the discharge capacity, because carbon limits the charge-transfer reaction at the surface of the alloy. In addition, Funaki et al. [18] prepared $MgNiC_x$ ($x = 0$–1.31) by mechanical alloying of amorphous MgNi and graphite for 20 h, and found that upon hydrogenation, the atomic ratio of hydrogen plus carbon to metal (H + C)/M in $MgNiC_x$ complex remained a constant value of about 0.9,

* Corresponding authors. Tel.: +86 532 85951961; fax: +86 532 85951519.
E-mail addresses: newboy66@126.com (H. Lin-jun), tang@qdu.edu.cn (T. Jian-guo).

indicating that carbon atoms dissolved into the sites that otherwise would be occupied by hydrogen atoms. Guo et al. [19] studied the effects of surface modification of amorphous $MgNi_{1+x}$ ($x = 0.05-0.3$) by introduction of various carbon sources in the system (graphite, CNTs and carbon black), and found that graphite could effectively increase the surface electrocatalytic activity and the cycle life of the electrodes.

Graphene, a 2D atomically thin film of carbon atoms, has unique characteristics that have triggered unprecedented research excitement [20]. Aside from the unique combination of strength and ductility, it also has remarkable chemical inertness such as resistance to HF [21]. Bunch et al. [22] has shown that graphene membrane can be impermeable to standard gases including helium. Additionally, graphene has a hydrophobic nature due to the non-polar covalent double bonds, which prevent hydrogen bonding with water [23]. Possessing the attributes of toughness and hydrophobicity, graphene has potential as an ultrathin protective coating especially in protection of metals from corrosion in marine or saline environment.

Silver (Ag) has good ductility, electric conductivity and thermal conductivity. Also Ag is a good catalyst for reduction of hydrogen in aqueous solution. The calculated results of Pozzo et al. [24] showed that Ag added to hydrogen storage alloys surface was conducive to their hydrogen absorption because of the convenient diffusion of hydrogen atoms in Ag surface. Qian et al. [25] prepared $Mg_{2-x}Ag_xNi$ ($x = 0.05, 0.1, 0.5$) alloys using hydrogenated burning way, founding that Ag can improve the absorption kinetics of hydrogen storage alloy. Thus, Ag is another ideal surface modification additive.

In our previous work, the crystallization, microstructure and hydrogen storage properties for various melt-spun Mg–Ni–RE (RE is a rare-earth element) and Mg–Cu–RE alloys were studied [26–30]. The amorphous structure was found to be the key factor to achieve a higher discharge capacity. However, little attention has been paid to the surface modification of amorphous alloy electrodes to improve their performance. An investigation on these would help to understand the hydrogen storage mechanism for amorphous alloys and improve their electrochemical properties.

Until now, there has no comparative study of the effects of graphene/Ag nanocomposite additives on electrochemical properties of Mg-based amorphous alloy. In this paper, melt-spun $Mg_{65}Ni_{27}La_8$ alloy was prepared and Ag nanoparticle have been deposited onto graphene sheets to form graphene/Ag (G/A) nanocomposite. The effect of surface modification on amorphous Mg–Ni–La electrode alloy by introduction of different contents of G/A was systematically investigated in detail.

2. Experimental

The Mg–Ni–La alloys ingot were prepared by melting a mixture of pure La metal and Mg–Ni intermediate alloy in a vacuum induction furnace under the protection of argon gas. The purity of the La metal and Mg–Ni intermediate alloy was 99.8 wt.% and 99.6 wt.%, respectively. Positive pressure protection and repeated melting were adopted to prevent serious evaporation of Mg and to ensure compositional homogeneity during the preparation of the master alloy ingot. The amorphous ribbons were produced using a single roller melt spinning technique (copper quenching disc with a diameter of 250 mm and surface velocity of about 39 m s^{-1}) in an argon atmosphere of 400 mbar. The as-quenched ribbons were then ball-milled into powder under the protection of an Ar atmosphere with a ball-to-powder weight ratio of 30:1 for 10 min using a specially made mill pot and an SPEX 8000 mill.

Natural graphite (carbon content: 99.9%) was purchased from Qingdao Aoke Co., China. Analytical-grade reagents, including silver nitrate ($AgNO_3$), ethylene glycol and absolute ethanol, were
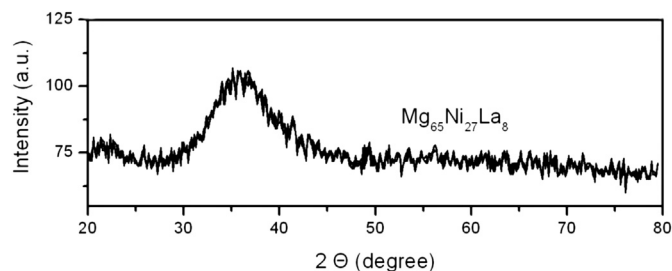

Fig. 1. X-ray diffraction patterns of the as-quenched $Mg_{65}Ni_{27}La_8$ amorphous alloy.

purchased from Sinopharm Chemical Reagent Co., Ltd., China, in analytical purity and used without further purification. Graphite oxide was prepared from purified natural graphite according to the method reported by Hummers and Offeman [31]. A 10 mg portion of graphite oxide powder was dispersed in 10 mL of water by sonication for 1 h, forming stable graphene oxide colloid. Then 20 mL of ethylene glycol and 100 mL $AgNO_3$ solution (0.1 mol L^{-1}) were added to the solution with magnetic stirring for 30 min. Subsequently, the mixture was put in an oil bath and heated at 100 °C for 6 h with magnetic stirring. The graphene with Ag nanoparticles were then separated from the ethylene glycol solution via centrifugation and washed with deionized water for five times. The resulting products were dried in a vacuum oven at 60 °C for 12 h.

The $Mg_{65}Ni_{27}La_8$ powder was then mixed with Ni powder and G/A powder with a mass ratio of 1:4:x ($x = 0, 0.1, 0.2, 0.3$) in a mortar. These mixtures were milled for another 3 min in the same condition for the surface modifications of $Mg_{65}Ni_{27}La_8$ powder. The $Mg_{65}Ni_{27}La_8$ alloy could retain the amorphous structure after 10 min of milling [18]. The test negative electrodes were fabricated by cold pressing the resultant powders into pieces of nickel foam under a pressure of 20 MPa. The electrodes were represented as $(Mg_{65}Ni_{27}La_8) + x$ G/A ($x = 0, 0.1, 0.2, 0.3$) based on the different G/A content.

The crystal structure of the G/A composites was characterized by a Philips 1730 powder X-ray diffractometer (XRD) with Cu Kα radiation. The morphology and microstructures were observed by a JEOL 6460 scanning electron microscope (SEM). High resolution transmission electron microscopy (HRTEM) was conducted on a JEOL 2011 transmission electron microscope (TEM) at an accelerating voltage of 200 kV. Infrared (IR) spectra of the samples were collected on a Nicolet Avatar 360 FTIR Fourier transform infrared (FTIR) spectrometer.

Electrochemical measurements were performed at room temperature (27 ± 1 °C) in 6 M KOH solution containing 20 g L^{-1} LiOH using a three-electrode cell. The positive and reference electrode were NiOOH/Ni(OH)$_2$ and Hg/HgO, respectively. Charge/discharge cycles were collected on an Arbin BT2000 battery tester. The electrode was charged at 100 mA g^{-1} for 10 h and discharged at 50 mA g^{-1}, and the cut-off potential was set at −0.5 V (versus Hg/HgO). The results were the average values from three parallel experiments to minimize the errors.

After the electrodes were completely activated by cycling, the anode polarization, linear polarization and electrochemical impedance spectroscopy (EIS) studies were conducted at 50% depth of discharge (DOD) using AMETEK Versa STAT MC electrochemical test system. The anode polarization and the EIS test were carried out at room temperature (27 ± 1 °C). The anode polarization and the linear polarization curves were measured by scanning the electrode potential at a rate of 5 mV s^{-1} from 0 to 600 mV (versus open circuit potential) and 0.1 mV s^{-1} from −5 to 5 mV (versus open circuit potential), respectively. The EIS measurements were

carried out in the frequency range of 10 kHz–5 mHz with an AC amplitude of 5 mV under the open circuit condition.

3. Results and discussions

Fig. 1 presents the X-ray diffraction patterns of the as-quenched $Mg_{65}Ni_{27}La_8$ alloy. It is seen that the melt-spun alloy show only a broad and diffuse peak. This suggests that the $Mg_{65}Ni_{27}La_8$ alloy prepared by melt-spinning is typical amorphous structure.

Fig. 2a gives the XRD patterns of various samples. As shown in Fig. 2a (a), there are no obvious diffraction peaks of graphite oxide or graphite were observed from the graphene XRD pattern. Recent studies [32] have shown that, if the regular stacks of graphite oxide or graphite are destroyed, for example, by exfoliation, their diffraction peaks became weak or even disappeared. It does not matter whether the existent carbon sheets was graphene oxide or graphene in these composites; it was confirmed that the regular layered structure of graphite oxide or graphite was destroyed. After the chemical reduction by solvothermal method, the graphene/Ag composite showed characteristic peaks at 38.1°, 44.3°, 64.4° and 77.4° with high intensity (Fig. 2 a (b)), which can be assigned to the (1 1 1), (2 0 0), (2 2 0) and (3 1 1) planes of the cubic Ag crystal (JCPDS No. 04-0783), indicating that graphene/Ag composite was successfully prepared during our experiments.

The as-obtained graphene-oxide and graphene/Ag composite samples were also analyzed by means of FTIR spectroscopy and the results are shown in Fig. 2b. The relatively broad peak at 3416 cm^{-1} and relatively sharp peak at 1623 cm^{-1} indicate that the samples contain adsorbed water. The peaks at 1403 cm^{-1} and 1053 cm^{-1} can be assigned to the deformation vibration of O–H and stretching vibration of C–O, respectively. Characteristic bands of C=O carbonyl stretching and C–O–C vibration located at 1733 cm^{-1} and 1221 cm^{-1} are very weak, indicating the small amount of these two functional groups [33]. After the solvothermal reduction, removal of oxygen-containing groups is clearly indicated by the disappearance of the most absorption bands as shown in Fig. 2b. TEM images of graphene/Ag composites (Fig. 2c) show the wide distribution of Ag particles ranging in the diameter of 10–30 nm. It can be observed that graphene sheets are decorated by Ag particles which are well separated with each other and randomly distributed. Fig. 2d is the high-resolution image of Ag particles reduced by ethylene glycol. The fringe spacing shown in the image is about 0.2052 nm, which agrees well with the (2 0 0) lattice plane reported in the JCPDS (No. 04-0783).

Fig. 3 shows the SEM images of Mg–Ni–La + x G/A particle (x = 0, 0.1, 0.2, 0.3) without Ni powder (Ni powder was not added here in order to see the whole status of the surface modification). It can be observed that the composites are more sparsely distributed on the alloy surface when x was 0.1, indicating the dosage of G/A is little; when x was 0.2, the composites covers the entire surface of the alloy particles, showing a uniform distribution and better surface modification. When x reached 0.3 there were spherical agglomerates observed on the surface of the alloy particles.

The variation of the discharge capacity of the different samples with the number of cycles is shown in Fig. 4. It can be observed that the discharge capacity is greatly improved by surface modification using G/A. The maximum discharge capacity of each electrode increases first and then decreases with increasing G/A content.
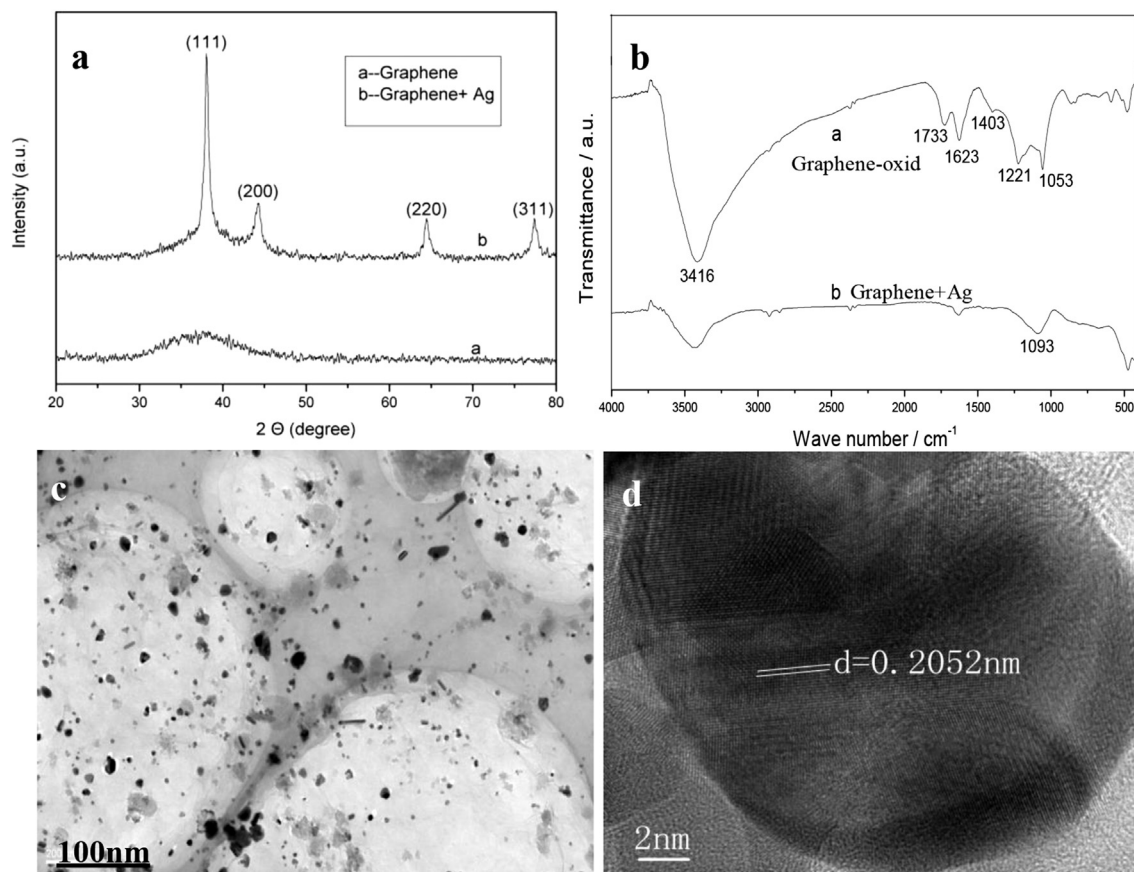

Fig. 2. XRD patterns of the graphene and graphene/Ag composites (a), FTIR spectra of graphene-oxide and as-prepared graphene/Ag composite (b), TEM image (c) and HRTEM image (d) of graphene/Ag composites.
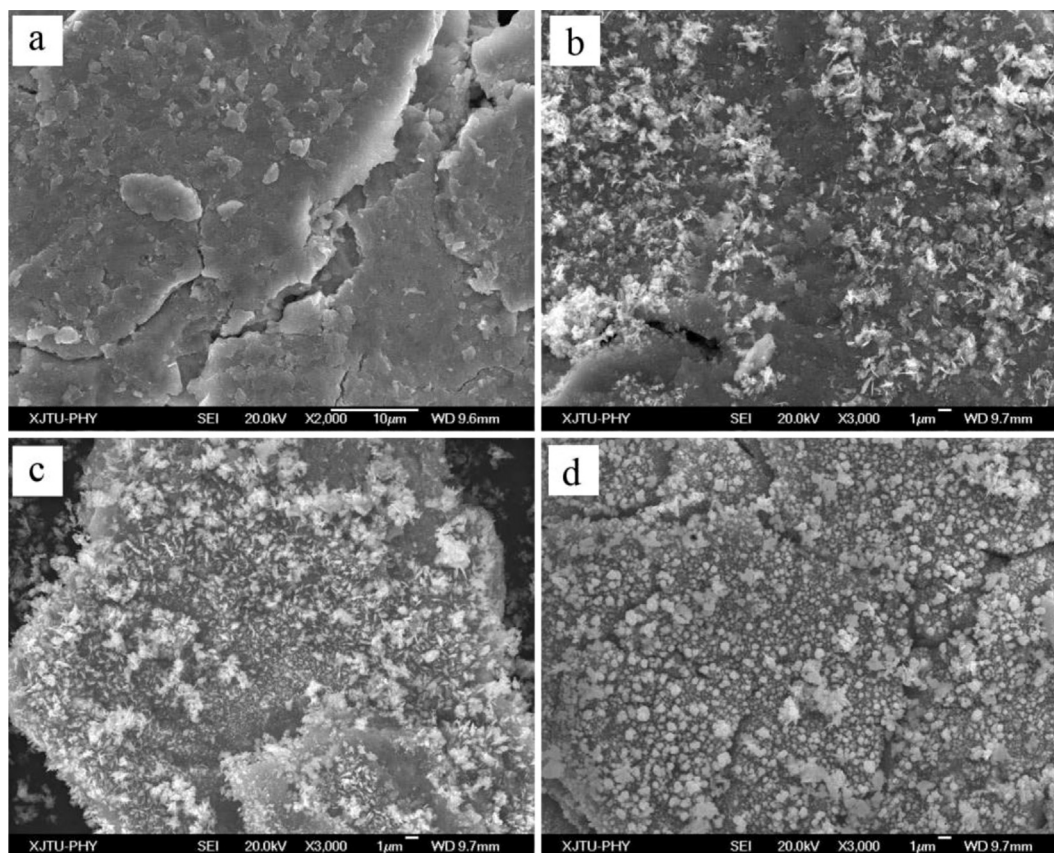
Fig. 3. SEM images of the surface of Mg–Ni–La + x G/A particle: $x = 0$ (a), $x = 0.1$ (b), $x = 0.2$ (c), $x = 0.3$ (d).

$Mg_{65}Ni_{27}La_8$ with 20 wt.% G/A exhibited the highest capacity and $Mg_{65}Ni_{27}La_8$ alone was the lowest one when they are activated. For each electrode, the discharge capacity reached a maximum after three or four cycles (activation period), and then decreases for more cycle numbers. The curves of the discharge capacity became smooth after 10 cycles. The largest discharge capacity reached 814.8 mAh g^{-1} for the samples with 20 wt.% G/A electrode, which is 1.33 times that obtained with G/A-free electrode, as shown in
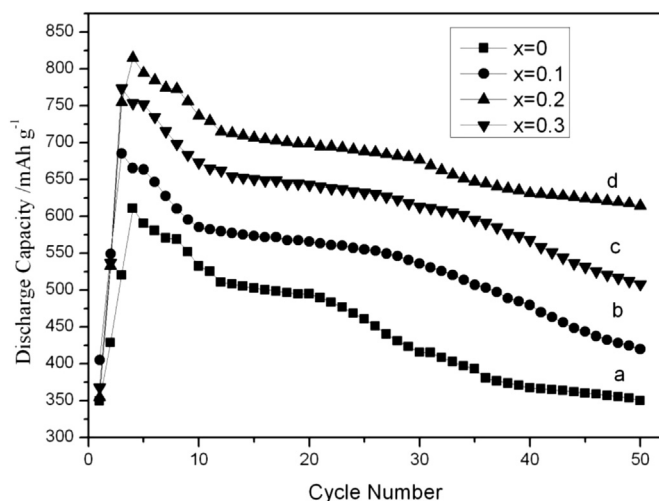
Table 1 (for the discharge capacity of $Mg_{65}Ni_{27}La_8$ alloy, only 4.7% data error was observed between this manuscript and the author's another paper [30]). Obviously, there is an optimal G/A content for the preparation of the amorphous Mg–Ni–La electrode with high discharge capacity. Table 1 also shows the activation period, the maximum capacity and capacity retention at the 20th cycle for different samples. The maximum discharge capacity of $Mg_{65}Ni_{27}La_8$ with 20 wt.% G/A electrode is higher than that of Mg–Ni–Nd alloys [26] and much higher than that of the AB_3 type alloys (about 400 mAh g^{-1}) [34,35]. A few reports about alloy modification with the single Ag also exist [36,37]. Wang and his co-workers found that the hydrogenation properties of $Mg_{1.8}Ag_{0.2}Ni$ alloy could be improved by inter-diffusion, such as absorbing hydrogen at low temperature (423 K) and prolonging the cycle life, but its maximum capacity only reached 2.8 mass% (about 777 mAh g^{-1}) at 573 K.

From above results, it is evident that the increase in discharge capacities is not only a function of the sample composition but also strongly influenced by the surface modification with G/A, The G/A composite can slightly expedite the process of activation and improve the capacity retention after 20 cycles, indicating the improvement of charge/discharge cycle life.

The relationship of discharge potentials (voltage) and the discharge capacities (at the 20 cycles) is shown in Fig. 5. It can be seen that the potential plateau becomes more horizontal with the increasing G/A content. The surface modification also decreases the discharge potential and increases the length of potential plateau compared to the G/A-free electrode, suggesting the decrease of hydrogen overpotential or the increase of the electrocatalytic activity.

Fig. 6 shows anode polarization curves of the $(Mg_{65}Ni_{27}La_8) + x$ G/A ($x = 0$–0.3) electrodes. In all cases, the anodic current densities

Fig. 4. Discharge capacities as a function of cycle number for the $(Mg_{65}Ni_{27}La_8) + x$ G/A ($x = 0$–0.3) negative electrodes.

Table 1
The activation period, the maximum discharge capacity (C_{max}), the discharge capacity after 20 cycles (C_{20}) and capacity retention for Mg–Ni–La + x G/A samples.

Samples	Activation period/cycle	C_{max}/mAh g^{-1}	C_{20}/mAh g^{-1}	Capacity retention/%
$x = 0$	4	610.8	487.8	79.86
$x = 0.1$	3	685.5	565.9	82.55
$x = 0.2$	4	814.8	698.8	85.76
$x = 0.3$	3	753.4	642.8	85.32

Table 2
Limiting current density I_L (27 °C) and the exchange current densities I_0 for the Mg–Ni–La + x G/A electrodes.

Samples	I_L/mA g^{-1}	I_0/mA g^{-1}
$x = 0$	2233.4	156.2
$x = 0.1$	2967.4	170.3
$x = 0.2$	5672.3	213.6
$x = 0.3$	4095.6	192.5
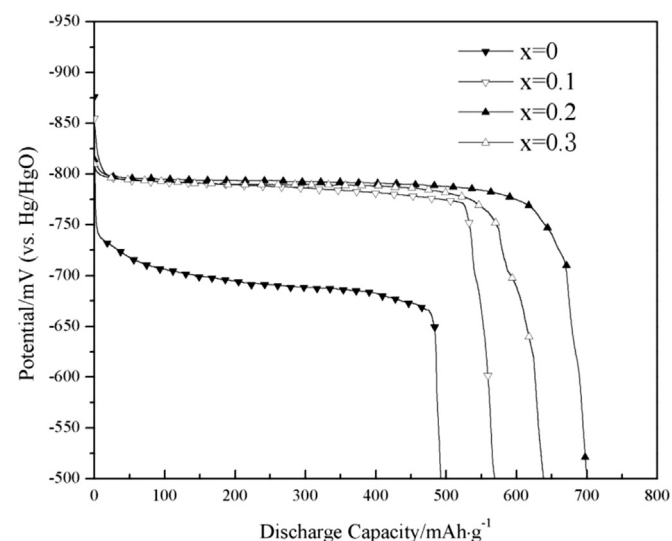
Fig. 5. Discharge potential curves of the (Mg$_{65}$Ni$_{27}$La$_8$) + x G/A (x = 0−0.3) electrodes at the 20th cycle.

increase to a limiting value and then decrease. The anodic peaks correspond to the oxidation of hydrogen, because they are measured at 50% DOD. The limiting current density I_L (an electrochemical kinetics parameter, meaning the speed of mass transfer process in the electrode reaction) is listed in Table 2. It increases first from 2233.4 mA g^{-1} ($x = 0$) to 5672.3 mA g^{-1} ($x = 0.2$) and then decreases to 4095.6 mA g^{-1} ($x = 0.3$), which implies the electrochemical kinetics of the electrodes increases first and then

decreases with increasing G/A content. This illustrates that the diffusion steps play a relatively small role in electrode reaction process for Mg$_{65}$Ni$_{27}$La$_8$ with 20 wt.% G/A electrode, which shows a relatively fast mass transfer process could better meet the needs for electrochemical reaction.

The exchange current densities I_0 for the electrodes are calculated using the following expression [38]:

$$I_0 = I_d \frac{RT}{F\mu} \qquad (1)$$

where R, T, I_d, F, μ are the gas constant, the absolute temperature, the applied current density, the Faraday's constant and the total over-potential, respectively. I_d/μ is the slope of these straight lines. Fig. 7 presents the linear polarization curves of the different electrodes. One of the biggest slope was observed with Mg$_{65}$Ni$_{27}$La$_8$ with 20 wt.% G/A electrode, followed by Mg$_{65}$Ni$_{27}$La$_8$ with 30 wt.% G/A electrodes, the smallest is G/A-free electrode. Corresponding exchange current density I_0 is listed in Table 2. Mg$_{65}$Ni$_{27}$La$_8$ with 20 wt.% G/A electrode exhibited the highest exchange current density of 213.6 mA g^{-1}, that implies its good polarization resistance and also explains why the discharge voltage of Mg$_{65}$Ni$_{27}$La$_8$ with 20 wt.% G/A electrode is lower than other electrodes.

Fig. 8 shows electrochemical impedance spectra of the different electrodes. Each spectrum consists of two semicircles in the high-frequency region followed by a straight line in the low-frequency region. According to literature [39], the small arc in the high-frequency region and the large arc in the low-frequency region can be assigned to the contact resistance (R_{cp}) between the current collector (Ni foam) and the alloy particles, and to the charge-transfer reaction resistance (R_{ct}) on the alloy surface, respectively. Using the equivalent circuit [40] as shown in Fig. 8, the values of four electrodes can be calculated. R_s, Z_w and $Q_{1(2)}$ in Fig. 8 represent
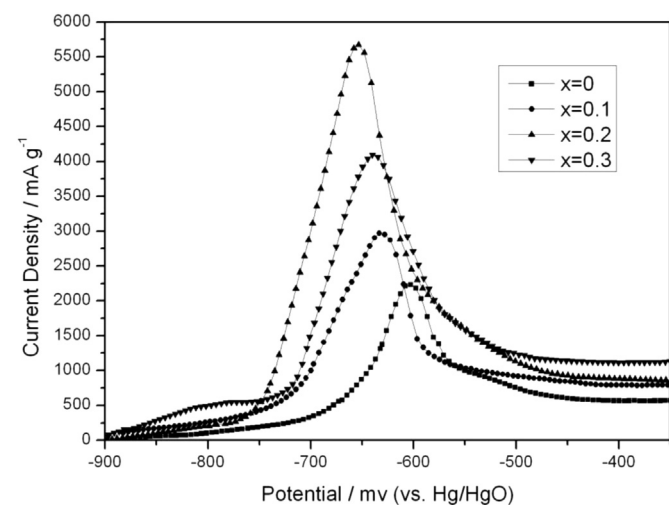

Fig. 6. Anode polarization curves of the (Mg$_{65}$Ni$_{27}$La$_8$) + x G/A (x = 0−0.3) electrodes at 50% depth of discharge at 27 °C.

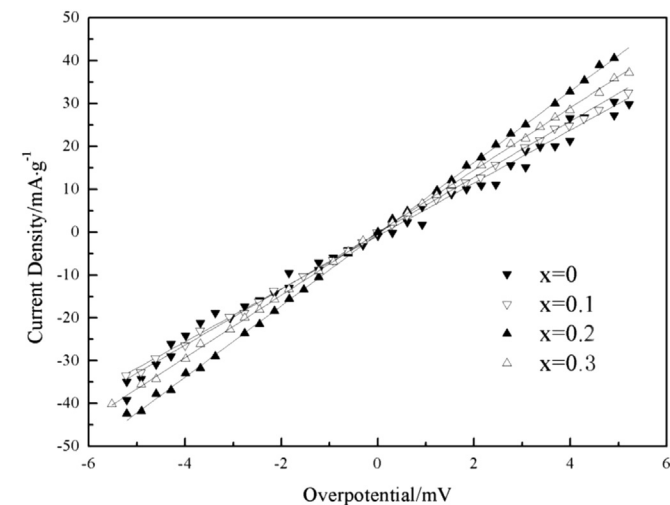**Fig. 7.** The linear polarization curves of the Mg–Ni–La + x G/A (x = 0−0.3) electrodes at 50% depth of discharge at 27 °C.
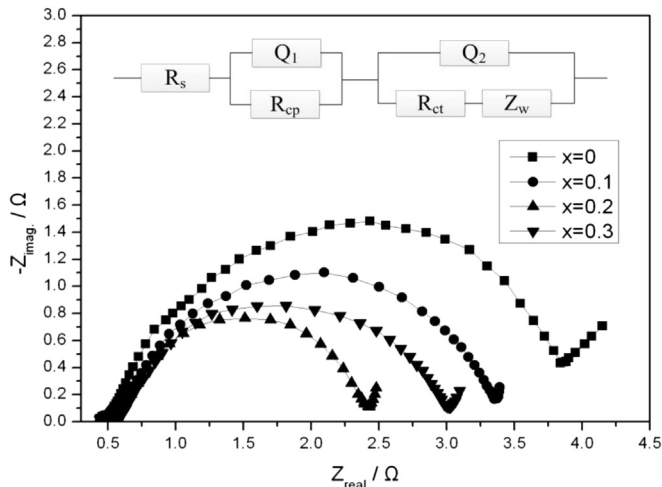
Fig. 8. Electrochemical impedance spectra of the Mg−Ni−La + x G/A (x = 0−0.3) electrodes at 50% depth of discharge at 27 °C. Inset is a photograph of equivalent circuit.

the solution resistance, the Warburg impedance, and the imperfect capacitor, respectively. The results are listed in Table 3. Both of the R_{cp} and R_{ct} decrease first and then increase with the increasing G/A content. The $Mg_{65}Ni_{27}La_8$ with 20 wt.% G/A electrode shows the lowest contact resistance and charge-transfer reaction resistance, suggesting the best electrochemical kinetics.

It is well-known that the practical application of Mg-based alloys is restrained by their poor charge/discharge cycle stability caused by the formation of $Mg(OH)_2$ on the surface of alloys in alkaline solution. The formation of $Mg(OH)_2$ will lead to the loss of hydrogen storage materials and obstructs the diffusion of hydrogen atoms as well [41]. Therefore, the increase of the anti-oxidation and anti-corrosion of the alloys seems to be an important factor to improve the electrode properties. If the alloy surface is covered with G/A, the condition will be different. It is expected that G/A will react with amorphous Mg−Ni−La alloy and probably donate electron to the alloy surface during high-energy ball milling. The electrons trapped on the alloy surface might change the chemical states of the interaction between Mg and G/A−Mg on the alloy surface and correspondingly increase the active sites for hydrogen absorption and desorption and partially prevent the formation of $Mg(OH)_2$ on the alloy surface. That would increase the anti-oxidation and anti-corrosion of the alloys and improve the cycle stability of the alloy electrodes.

According to the above results, the influence of the surface modification of amorphous $Mg_{65}Ni_{27}La_8$ electrodes with G/A on the electrochemical characteristics could be illuminated as follows: (1) The surface modification could enhance the electrocatalytic activity of the alloy, reduce the contact resistance of the electrodes, and also increase the anti-oxidation and anti-corrosion performance of the alloys. Thus, the electrochemical properties of amorphous

$Mg_{65}Ni_{27}La_8$ electrodes are improved. (2) The performance of the $Mg_{65}Ni_{27}La_8$ with 30 wt.% G/A electrode is worse than that of the $Mg_{65}Ni_{27}La_8$ with 20 wt.% G/A electrode in almost every aspect. This is considered to be caused by two reasons. Firstly, the gaps between $Mg_{65}Ni_{27}La_8$ powder and Ni powder are limited. When the G/A content exceeds a certain value, the G/A composite will become thick and aggregated, and lead to the increase of contact resistance (refer to Table 3). Secondly, further increase of G/A composite thickness will make the diffusion of hydrogen atoms more difficult, leading to a decrease of electrode properties.

4. Conclusions

The electrochemical characteristics of amorphous $Mg_{65}Ni_{27}La_8$ electrode are greatly improved by surface modification using different contents of G/A composite. The surface modification could enhance the electrocatalytic activity of the alloy, reduce the contact resistance of the electrodes, and also increase the anti-oxidation and anti-corrosion performance of the alloys. Therefore, the discharge capacity, limiting current density, discharge potential characteristics and cycle life of the electrodes can be improved. An optimal content of 20 wt.% G/A in alloy composite has been obtained. The $Mg_{65}Ni_{27}La_8$ with 20 wt.% G/A electrode exhibited the largest discharge capacity of 814.8 mAh g^{-1} and the best electrochemical kinetics among the studied electrodes. Further increase of the G/A content will compromise the performance of the electrode.

References

[1] F.C. Gennari, F.J. Castro, G. Urretavizcaya, G. Meye, J. Alloys Compd. 334 (2002) 277−282.
[2] J.F.R. de Castro, S.F. Santos, A.L.M. Costa, A.R. Yavari, W.J. Botta, F.T.T. Ishikawa, J. Alloys Compd. 376 (2004) 251−256.
[3] C.X. Shang, M. Bououdina, Y. Song, Z.X. Guo, Int. J. Hydrogen Energy 29 (2004) 73−79.
[4] J.F. Pelletier, J. Huot, M. Sutton, R. Schulz, A.R. Sandy, L.B. Lurio, S.G.J. Mochrie, Phys. Rev. B 63 (2001) 521−524.
[5] J. Charbonnier, P. de Rango, D. Fruchart, S. Miraglia, L. Pontonnier, S. Rivoirard, N. Skryabina, P. Vulliet, J. Alloys Compd. 383 (2004) 205−212.
[6] A.R. Yavari, A. LeMoulec, F.R. de Castro, S. Deledda, O. Friedrichs, W.J. Botta, G. Vaughan, T. Klassen, A. Fernandez, A. Kvick, Scr. Mater. 52 (2005) 719−723.
[7] I.G. Konstanchuk, E.Y. Ivanov, M. Pezat, B. Darriet, V.V. Boldyrev, P. Hagenmuller, J. Less-Common Met. 131 (1987) 181−187.
[8] Z. Dehouche, T. Klassen, W. Oelerich, J. Goyette, T.K. Bose, R. Schulz, J. Alloys Compd. 347 (2002) 319−325.
[9] J.L. Bobet, F.J. Castro, B. Chevalier, Scr. Mater. 52 (2005) 33−37.
[10] F.J. Castro, J.L. Bobet, J. Alloys Compd. 366 (2004) 303−309.
[11] H. Imamura, S. Tabata, N. Shigetomi, Y. Takesue, Y. Sakata, J. Alloys Compd. 330−332 (2002) 579−586.
[12] C.X. Shang, Z.X. Guo, J. Power Sources 129 (2004) 73−78.
[13] D. Chen, L. Chen, S. Liu, C.X. Ma, D.M. Chen, L.B. Wang, J. Alloys Compd. 372 (2004) 231−236.
[14] C. Iwakura, H. Inoue, S.G. Zhang, S. Nohara, J. Alloys Compd. 293−295 (1999) 653−657.
[15] S. Nohara, H. Inoue, Y. Fukumoto, C. Iwakura, J. Alloys Compd. 252 (1997) L16−L18.
[16] C. Iwakura, H. Inoue, S. Nohara, R. Shin-ya, S. Kurosaka, K. Miyanohara, J. Alloys Compd. 330−332 (2002) 636−639.
[17] S. Ruggeri, L. Roué, G. Liang, J. Huot, R. Schulz, J. Alloys Compd. 343 (2002) 170−178.
[18] K. Funaki, S. Orimo, H. Fujii, H. Sumida, J. Alloys Compd. 270 (1998) 160−163.
[19] Z.P. Guo, Z.G. Huang, K. Konstantinov, H.K. Liu, S.X. Dou, Int. J. Hydrogen Energy 31 (2002) 2032−2039.
[20] A.K. Geim, K.S. Novoselov, Nat. Mater. 6 (2007) 183−191.
[21] E. Stolyarova, D. Stolyarov, K. Bolotin, S. Ryu, L. Liu, K.T. Rim, Nano Lett. 9 (2012) 332−337.

Table 3
Contact resistance R_{cp} and charge-transfer resistance R_{ct} of the Mg−Ni−La + x G/A electrodes at 27 °C.

Samples	R_{cp}/mΩ	R_{ct}/Ω
x = 0	917	3.08
x = 0.1	163	2.86
x = 0.2	117	1.77
x = 0.3	154	2.41

[22] J.S. Bunch, S.S. Verbridge, J.S. Alden, AMvd Zande, J.M. Parpia, H.G. raighead, Nano Lett. 8 (2008) 2458–2462.
[23] O. Leenaerts, B. Partoens, F.M. Peeters, Phys. Rev. B 79 (2009) 235–240.
[24] M. Pozzo, D. Alfe, Int. J. Hydrogen Energy 4 (2009) 1922–1930.
[25] L. Qian, L. Qin, J. Lijun, J. Alloys Compd. 359 (2003) 128–132.
[26] L.J. Huang, G.Y. Liang, Z.B. Sun, J. Power Sources 160 (2006) 684–687.
[27] L.J. Huang, G.Y. Liang, Z.B. Sun, Y.F. Zhou, J. Alloys Compd. 432 (2007) 172–176.
[28] L.J. Huang, Jian-guo Tang, G.Y. Liang, Yao Wang, D.C. Wu, J. Power Sources 189 (2009) 1247–1250.
[29] L.J. Huang, Jian-guo Tang, Yao Wang, Ji-xian Liu, D.C. Wu, J. Alloys Compd. 485 (2009) 186–191.
[30] L.J. Huang, Yan-xin Wang, D.C. Wu, Jian-guo Tang, Yao Wang, Ji-xian Liu, Zhen Huang, Jing-quan Liu, J. Power Sources 249 (2014) 35–41.
[31] W. Hummers, R. Offeman, J. Am. Chem. Soc. 80 (1958) 1339–1343.
[32] C. Xu, X.D. Wu, J.W. Zhu, X. Wang, Carbon 46 (2008) 386–391.
[33] S. Stankovich, R.D. Piner, S.T. Nguyen, R.S. Ruoff, Carbon 44 (2006) 3342–3349.
[34] H.G. Pan, Y.F. Liu, M.X. Gao, Intermetallics 13 (2005) 770–778.
[35] F.L. Zhang, Y.C. Luo, J.P. Chen, J. Power Sources 150 (2005) 247–254.
[36] G. Liang, J. Hout, S. Boily, J. Alloys Compd. 282 (1999) 286–289.
[37] Lian-bang Wang, Yuan-hua Tang, Yi-jing Wang, Qiu-Di Li, He-nan Song, Hua-bin Yang, J. Alloys Compd. 336 (2002) 297–300.
[38] P.H.L. Notten, P. Hokkeling, J. Electrochem. Soc. 138 (1991) 1877–1885.
[39] N. Kuriyama, T. Sakai, H. Miyamura, I. Uehara, H. Ishikawa, T. Iwasaki, J. Alloys Compd. 202 (1993) 183–197.
[40] Q. Liu, L.F. Jiao, H.T. Yuan, Y.J. Wang, Y. Feng, J. Alloys Compd. 427 (2007) 275–280.
[41] W. Liu, Y. Lei, D. Sun, J. Wu, Q. Wang, J. Power Sources 58 (1996) 243–247.